

alkali series. However, it must be remembered that the approximation of treating changes in one type of force constant as independent of the changes in the others is not precise.

Acknowledgments: The author is very grateful to Prof. Navrotsky for ungrudging help and support during this work and Dr. R. Nieman for his advice in the use of the FT-IR spectrometer. Dr. P. McMillan supplied the crystalline rubidium.

References

- ¹B. N. Roy and A. Navrotsky, "Thermochemistry of Charge-Coupled Substitutions in Silicate Glasses: The Systems $M_{1-x}^{2+}AlO_2-SiO_2$ ($M = Li, Na, K, Rb, Cs, Mg, Ca, Sr, Ba, Pb$)," *J. Am. Ceram. Soc.*, **67** [9] 606-10 (1984).
- ²V. A. Kolesova, "Infrared Absorption Spectra of Low-Alkali and Alkali-Free Aluminosilicate Glasses," *Izv. Akad. Nauk SSSR, Neorg. Mater. (Engl. Transl.)*, **1** [3] 442-45 (1965).
- ³I. Simon and H. O. McMahon, "Study of Some Binary Silicate Glasses by Means of Reflection in Infrared," *J. Am. Ceram. Soc.*, **36** [5] 160-64 (1953).
- ⁴R. Hanna and G.-J. Su, "Infrared Absorption Spectra of Sodium Silicate Glasses from 4 to 30 μm ," *J. Am. Ceram. Soc.*, **47** [12] 597-601 (1964).
- ⁵P. E. Jellyman and J. P. Proctor, "Infrared Reflection Spectra of Glasses," *J. Soc. Glass Technol.*, **39**, 173-92 (1955).
- ⁶V. A. Florinskaya and R. S. Pechenkina, "Spectra of Simple Glasses in the Infrared Range and Their Relations to the Structure of Glass: III. Structure of Sodium Silicate Glasses," *Glass Ind.*, **39** [3] 151-54 (1958) (translated from Russian text by Wilhelm Eitel).
- ⁷M. K. Murthy and E. M. Kirby, "Infrared Study of Compounds and Solid Solutions in the System Lithia-Alumina-Silica," *J. Am. Ceram. Soc.*, **45** [7] 324-29 (1962).
- ⁸P. Launer, "Regularities in the Infrared Absorption Spectra of Silicate Minerals," *Am. Mineral.*, **37**, 764-84 (1952).
- ⁹T. A. Sidorov, "Study of the Infrared Reflection Spectra of Lithium-Aluminum-Silicate Glasses and Glass-Ceramic Compounds," *Zh. Prikl. Spektrosk.*, **5** [1] 111-17 (1966).

- ¹⁰D. E. Day and G. E. Rindone, "Properties of Soda Aluminosilicate Glasses: I. Refractive Index, Density, Molar Refractivity, and Infrared Absorption Spectra," *J. Am. Ceram. Soc.*, **45** [10] 489-96 (1962).
- ¹¹V. A. Kolesova, "Infrared Absorption Spectra of the Silicates," *Opt. Spectrosc.*, **6** [1] 20-24 (1959).
- ¹²P. Tarte, "The Determination of Cation Coordination in Glass by Infrared Spectroscopy," *Proc. Int. Conf. Phys. Non-Cryst. Solids, Delft, The Netherlands*, 549-65 (1964).
- ¹³P. Tarte, "Infrared Spectroscopic Study of Orthosilicates and Orthogermanates. A Novel Method of Interpretation of Spectra" (in Fr.), *Spectrochim. Acta*, **18**, 467-83 (1962).
- ¹⁴V. C. Farmer, "The Infrared Spectra of Minerals"; in Mineralogical Society Monograph 4. Edited by V. C. Farmer. Mineralogical Society, London, 1974.
- ¹⁵B. D. Saksena, K. C. Agarwal and G. S. Jauhri, "The Ring Band of Cyclo-Silicates," *Trans. Faraday Soc.*, **59**, 276-83 (1963).
- ¹⁶W. B. White, "Structural Interpretation of Lunar and Terrestrial Minerals by Raman Spectroscopy"; Ch. 13 in *Infrared and Raman Spectroscopy of Lunar and Terrestrial Minerals*. Edited by Clarence Karr, Jr. Academic Press, New York, 1975.
- ¹⁷S. A. Braver and W. B. White, "Raman Spectroscopic Investigation of the Structure of Silicate Glasses. I. The Binary Alkali Silicates," *J. Chem. Phys.*, **63** [6] 2421-32 (1975).
- ¹⁸S. A. Braver and W. B. White, "Raman Spectroscopic Investigation of the Structure of Silicate Glasses. II. Soda-Alkaline-Earth-Alumina Ternary and Quaternary," *J. Non-Cryst. Solids*, **23**, 261-78 (1977).
- ¹⁹J. M. Bates, "Dynamics of β -Quartz Structures of Vitreous SiO_2 and BeF_2 ," *J. Chem. Phys.*, **56**, 1910-17 (1972).
- ²⁰P. Tarte, "Identification of Li-O Bands in the Infrared Spectra of Simple Lithium Compounds Containing LiO_4 Tetrahedra," *Spectrochim. Acta*, **20**, 238-40 (1964).
- ²¹L. A. Ignat'eva, "Study of α - and β -Spodumene by Infrared Spectroscopy," *Opt. Spectrosc.*, **6** [6] 527-29 (1959).
- ²²W. Gordy, "A Relation between Bond Force Constants, Bond Orders, Bond Lengths, and Electronegativities of the Bonded Atoms," *J. Chem. Phys.*, **14**, 305-20 (1946).
- ²³R. G. Milkey, "Infrared Spectra of Some Tectosilicates," *Am. Mineral.*, **45**, 990-1007 (1960).
- ²⁴W. A. Weyl and E. C. Marboe in *The Constitution of Glasses*, Vol. I. Interscience, New York, 1961; Vol. II, 1964. □

J. Am. Ceram. Soc., **70** [3] 192-96 (1987)

Diffraction Studies of a Highly Metastable Form of Amorphous Silica

JOHN KONNERT and PETER D'ANTONIO

Naval Research Laboratory, Washington, D.C. 20375

MARIA HUFFMAN*

General Electric Co., Worthington, Ohio 43085

ALEXANDRA NAVROTSKY*

Department of Geological and Geophysical Sciences, Princeton University, Princeton, New Jersey 08544

An amorphous powder of SiO_2 that calorimetric studies indicated to be energetically metastable by 46.9 ± 0.8 kJ/mol relative to fused silica was studied by X-ray diffraction. A calculation of the energetic instability, based on the bond length and bond angle distributions derived from the diffraction data and utilizing the force constants for bond stretching and bending, indicated that 41.3 ± 7.9 kJ/mol of the instability may be associated with distortions of the Si-O bonds, the O-Si-O bond angles, and the Si-O-Si angles. Analyses of the extensive small-angle scattering from the porous material suggested that only a small portion of the instability is associated with surface structures.

Received March 13, 1986; revised copy received September 12, 1986; approved October 2, 1986.

Supported in part by the National Science Foundation under Grant No. DMR 8211127.

*Member, the American Ceramic Society.

I. Introduction

CALORIMETRIC studies have been performed on a powder ("snow") of SiO_2 deposited in the cool ends of furnace tubes used for coating silicon wafers with amorphous SiO_2 films by low-pressure chemical vapor deposition (LPCVD) used in semiconductor technology.¹ The studies indicated this amorphous material to be metastable by as much as 46.9 kJ/mol relative to fused silica. The diffraction studies reported here were undertaken to correlate structure on the atomic level with this instability. Unlike fused silica² this material exhibits extensive small-angle scattering. The small-angle data were collected and analyzed to yield estimates of the size distribution of voids present in the sample and the fraction of the atoms that could be associated with surface structure around these voids. High-angle scattering information was also collected, and, from it, the radial distribution function (RDF) that indicates the values and frequency of occurrence of interatomic distances was obtained. This RDF was compared to the one for

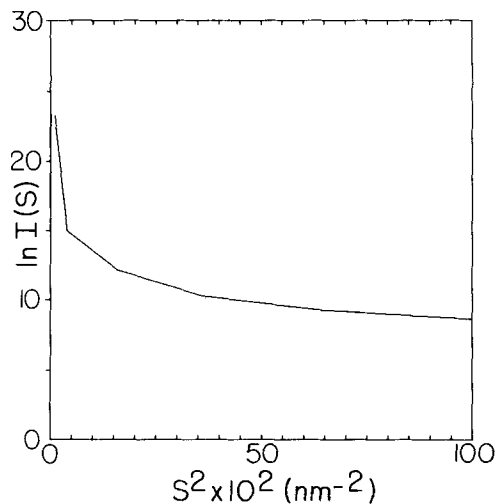


Fig. 1. Guinier plot of the small-angle X-ray scattering of snow silica.

fused silica. The differences, combined with simple force constants for bond deformations, were used to estimate the excess potential energy stored in strained bond distances and angles.

II. Experimental Procedure and Discussion

(1) Sample Preparation

One of the major methods of obtaining amorphous thin films is low-pressure chemical vapor deposition (LPCVD).¹ Two kinds of samples can be obtained from a hot-wall LPCVD furnace, thin films heterogeneously deposited on a substrate in the central hot zone and homogeneously deposited "snow," the latter being a very reactive powder adhering to the furnace walls at the cooler ends of the deposition tube. The deposition system used for sample preparation is described elsewhere.³ The gases used were SiH_4 and O_2 , which react in the hot reaction chamber to produce amorphous SiO_2 . The snow sample in this study was collected during a 703 K deposition run (temperature range at ends of furnace was 344 to 673 K).

(2) Low-Angle X-ray Data

The material was packed into a thin-walled glass capillary 1 mm in diameter. Data were collected in the range $0.01 < s < 3 \text{ nm}^{-1}$ in increments of 0.01 with a Kratky camera equipped with a diffracted beam monochromator using $\text{CuK}\alpha$ ($\lambda = 0.154 \text{ nm}$) radiation. Here $s = 4\pi \sin \theta / \lambda$, where 2θ is the angle between the incident and scattered beams. The scattering from the capillary, which rises slowly from zero at $s = 0$, was subtracted with appropriate consideration for absorption. The intensity was placed on an absolute scale by measuring the scattering from a calibrated film of polyethylene.⁴

(3) High-Angle X-ray Data

The material was packed into a 5 mm by 30 mm by 1 mm sample holder. Thin (0.013 mm) mylar was fixed over each 5 mm by 30 mm face to form a flat sample suitable for transmission measurements. Data were collected in the range $2 < s < 160 \text{ nm}^{-1}$ in increments of 0.5 using $\text{AgK}\alpha$ radiation ($\lambda = 0.054 \text{ nm}$), pinhole collimation (1° divergence), diffracted beam monochromator, and pulse height analyzer. Similarly, data were collected for the mylar only and its contribution from the first experiment was subtracted after suitable absorption corrections. Lorentz and polarization corrections were made.

(4) Analyses of Low-Angle Data

Extensive small-angle scattering (SAS) was observed. The scattering of X-rays is sensitive to fluctuations in the electron density

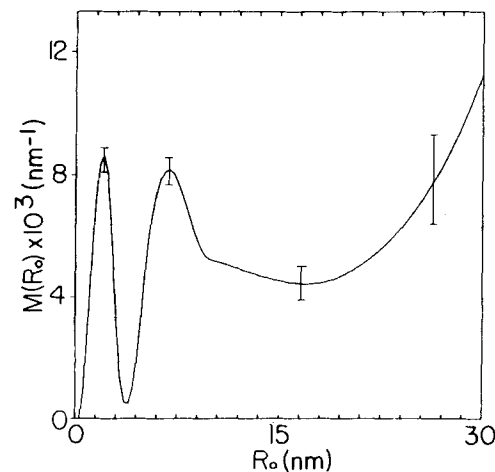


Fig. 2. Fractional void volume distribution for snow silica. Error bars are standard deviations obtained from least-squares fit of small-angle scattering.

of the material. The SAS is determined by such inhomogeneities of electron density in regions measuring $\approx 0.6 \text{ nm}$ or greater in size. The inhomogeneities may be the result of phase separation, the presence of small voids, the presence of small particles, or a combination.

The inhomogeneities were assumed to be voids in the following analyses. Phase separation in essentially pure SiO_2 is not possible; thus the presence of particles of a different composition appears unlikely. A portion of the small-angle scattering could also arise from small silica particles rather than voids. However, since the surfaces of voids and particles involve approximately the same number of atoms, conclusions concerning surface area will not be altered by the presence of both voids and particles. In the approximation that such regions are widely dispersed and the approximate law of Guinier⁵ holds, the scattering is proportional to

$$I_c(s) \propto \int R_0^3 M(R_0) e^{-s^2 R_0^2} dR_0 \quad (1)$$

where $I_c(s)$ is the calculated intensity, $M(R_0)$ is the volume fraction of the inhomogeneities with radius of gyration R_0 . For a spherical region $R_0^2 = 0.6R^2$, where R is the radius of the sphere. It can be seen from Eq. (1) that a plot of the natural logarithm of the intensity vs. s^2 (Guinier plot) will be a straight line if only a single size region is present. A Guinier plot of the small-angle scattering corrected for slit geometry aberrations is shown in Fig. 1. The nonlinearity indicates a distribution of inhomogeneity sizes.

The volume fraction, $M(R_0)$, in Eq. (1) was expressed as a flexible function whose shape was altered with a least-squares procedure to reproduce the observed intensity as closely as possible. Figure 2 illustrates the void volume distribution obtained. Correction for the broadening effects of the slit geometry are included in the refinement. Integration over this function yields the void volume fraction, x_v .

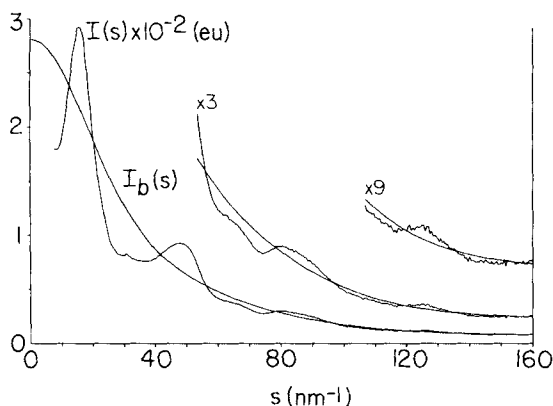
$$x_v = \int M(R_0) dR_0 = 0.16 \quad (2)$$

Thus, 16% of the sample volume is composed of voids of the size to which the experiment is sensitive. $M(R_0)$ indicates the presence of a number of voids with a radius of gyration of $R_0 = 2.1 \text{ nm}$ or a radius for the spherical voids of $R = 2.7 \text{ nm}$. Another peak is at $R = 8.9 \text{ nm}$. Other voids of larger size are indicated out to the limit of resolution which is $\approx 30.0 \text{ nm}$.

If the small-angle scattering could be separated from the high-angle data, then the surface area could be estimated from the shape of the tail of the small-angle scattering. Such a separation is not possible with the snow data. It is possible, however, to estimate the

Table I. Results of Analyses of Snow Silica by Small-Angle Scattering

Void radius (nm)	Void volume fraction	Fraction of atoms within 0.3 nm of surface
0–7.5	0.033	0.0067
0–15.0	0.062	0.0086
0–22.5	0.093	0.0098
0–30.0	0.159	0.0115

**Fig. 3.** Total X-ray diffraction pattern for snow silica, I_t , corrected for absorption and polarization, and the final representation for the background intensity, I_b .

fraction of atoms associated with the surface of these voids by calculating the number of atoms contained within a shell at the surface of the assumed spherical regions. Table I summarizes the results when all atoms within 0.3 nm of the surface of the voids indicated in Fig. 2 are designated as surface atoms. A total of 1.2% of the atoms are in this way associated with surfaces of voids detected by the small-angle scattering. It should be noted that, while Fig. 2 suggests the existence of voids larger than those detectable in this experiment, the majority of the surface atoms are associated with the smaller voids because the smaller spheres have larger surface-to-volume ratios.

The Si–O bond energy is ≈ 368 kJ/mol.¹¹ If 1.2% of the SiO_2 , residing near the surface, have all their bonds broken, the excess energy would be $(0.012)(2)(368)$ kcal = 17.6 kJ/mol. It is more likely that the structure near the voids has perhaps one Si–O–Si bond in four ruptured (analogous to a sheet silicate) with the Si–O then neutralized by hydrogen-bearing species CH_3^+ , H_3O^+ , H_2O , OH^- , etc., at the surface. The actual energy associated with these surface structures would then be much smaller, perhaps by 1 order of magnitude or more. Thus, it appears that the observed instability of ≈ 47 kJ/mol cannot be solely associated with surface atoms.

Low-resolution scanning electron microscopy has shown that, in general, snow silica CVD samples have a very open structure.³ In addition to overall small particle size, complex morphology is indicated, with each particle having a larger surface area than that of a smooth sphere of similar dimensions. While the voids or particles studied with the X-ray data are much smaller than those seen in SEM, these observations emphasize that the assumption of spherical voids or particles in the sample should be made with caution. Nevertheless, we conclude that the excess energy associated with surface species is of the order of 10 kJ/mol at most.

(5) Analyses of High-Angle Data

We now look at the structural properties of the bulk material for evidence related to the observed instability. This is accomplished by analyzing the high-angle scattering data. The diffraction pattern, I_t , shown in Fig. 3 may be expressed as a sum of components.

Table II. Short-Distance Parameters (r) and Their Rms (l) Displacement Amplitudes for Fused Silica and Snow*

	Fused	Snow
$r_{\text{Si-O}}$	0.1608 (2)	0.1611 (2)
$l_{\text{Si-O}}$	0.0056 (3)	0.0067 (4)
$r_{\text{O-O}}$	0.2632 (6)	0.2604 (8)
$l_{\text{O-O}}$	0.0097 (6)	0.0119 (7)
$r_{\text{Si-Si}}$	0.3085 (15)	0.3082 (15)
$l_{\text{Si-Si}}$	0.0100 (8)	0.0130 (10)

*All distances in nanometers; least-squares standard deviation in last place in parentheses.

$$I_t(s) = I(s) + I_b(s) \quad (3)$$

where $I(s)$ is the interference term and contains the interatomic distance information. $I_b(s)$ is the smooth background function that includes coherent and incoherent atomic scattering as well as instrumental background. In order to obtain the interatomic distance information, $I(s)$ must be isolated from $I_t(s)$ by subtracting $I_b(s)$. The interatomic distance distribution or radial distribution function (RDF) may be obtained from $I(s)$ by means of the Fourier sine transform

$$rG(r) = 4\pi r^2[\rho(r) - \rho_0] = \frac{2r}{\pi} \int_0^\infty s i(s) \sin sr ds \quad (4)$$

where $i(s) = [I_t(s) - I_b(s)]/\sum f^2(s)$, $\rho(r)$ represents the probability of occurrence of an interatomic distance within the range r and $r + dr$, ρ_0 is the bulk density averaged over the volume to which the experiment is sensitive, and $\sum f^2$, a sharpening function, is the sum of the squares of the atomic scattering factors for the unit of composition (SiO_2). The integral in Eq. (4) requires that $I(s)$ be known in the range $0 < s < \infty$, whereas it is only measured over a finite interval whose maximum is experimentally limited. Thus, in order to obtain an accurate RDF, $I(s)$ must be isolated from the total intensity and the effects of the termination of data must be minimized. This may be accomplished by collecting data with an appropriately small wavelength, and with data reduction techniques that require the resultant RDF to meet certain physical criteria.⁶

The treatment of the termination of the integral in Eq. (3) is based on the recognition that generally only the shortest distances make a significant contribution to the experimental intensity function, $i(s)$, beyond the measured range of scattering angle due to their small thermal or disorder parameters. Because of this, the data reduction procedure⁶ yields accurate parameters for the short distances. Table II lists the short-distance parameters obtained along with those obtained for bulk fused silica. The Si–O bond distributions are centered at essentially the same value of 0.161 nm, but the snow silica has an rms amplitude of disorder ≈ 0.002 nm larger. The O–O distribution for snow silica is not only 0.003 nm broader but also is centered at 0.260 nm, 0.003 nm shorter than for fused silica. The Si–Si distribution is also 0.003 nm broader for snow, but centered to within experimental error at the same value as for bulk glass.

The reduced intensity function for snow silica is illustrated in Fig. 4 along with the corresponding function for bulk silica glass. The RDFs for snow silica and bulk silica are compared in Fig. 5.

The RDFs are very different. They may be compared by calculating a correlation function, $F(g, h)$, between curves g and h .

$$F(g, h) = \int [rG_g(r)][rG_h(r)] dr / \left(\int [rG_g(r)]^2 dr \int [rG_h(r)]^2 dr \right)^{1/2} \quad (5)$$

This function may range in value from 1 to -1 . A value of 1 corresponds to perfect positive correlation, whereas a value of zero corresponds to no correlation.

Table III gives the correlation coefficients comparing the two RDFs. Not only do the amplitudes of the oscillations fall off much

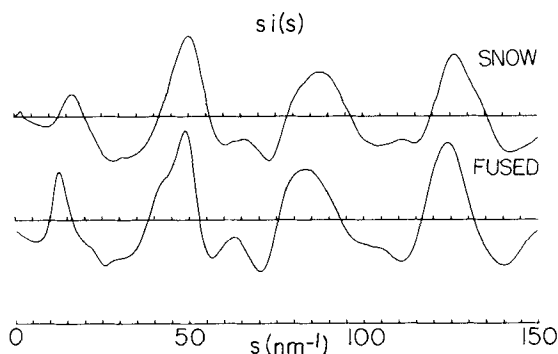


Fig. 4. Reduced intensity functions, $s_i(s)$, for snow and fused silica.

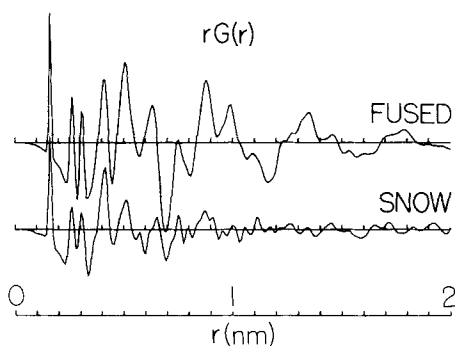


Fig. 5. Radial distribution functions for snow and fused silica.

more rapidly for the snow silica, but the maxima around 0.6 nm occur at quite different r values. The large differences in the two curves in the 0.4- to 0.6-nm region with regard to both amplitudes and position indicate that the ring statistics are very different for the two phases. Six-membered rings of silicate tetrahedra appear to be favored in the bulk silica.⁷ Very possibly the differences in the 0.4 to 0.6-nm region indicate the presence of more rings of different size. The absence of significant oscillations in the snow silica beyond 1.0 nm indicates much less long-range order than is present in bulk silica which possesses significant oscillations out to at least 2.0 nm.

Table IV lists the correlation coefficients comparing the two reduced intensities. Large differences are particularly noticeable around the s values of 15 and 85.

(6) Relation of Observed Distance Distributions to Potential Energy

The widths of the Si-O, O-O, and Si-Si distance distributions were used to estimate the potential energy that is associated with observed distortions of bond distances and angles from equilibrium values for bulk glass. Each observed distance distribution was assumed to be the convolution of a thermal motion distribution with a positional disorder distribution. Equivalently, the variance of the observed distribution (l^2) is taken as the sum of the variances of the thermal (l_T^2) and disorder (l_D^2) distributions. The normal modes of vibration that describe the thermal motion of the system were taken as also representing the displacement distributions necessary to describe the positional disorder in the glasses. Normal coordinate calculations were carried out using a program written by Kuhl and Hildebrand⁸ using force constants from Gibbs⁹ on a 30-atom group taken from terrestrial low tridymite (a crystalline polymorph of silica with 240 atoms in the asymmetric unit).¹⁰ Summation of the force constants associated with all of the modes suggested that each SiO₂ group has associated with it ap-

Table III. Correlation of Fused Silica and Snow Silica Radial Distribution Functions, $rG(r)$

Range (nm)	Correlation
0.0-1.0	0.79
1.0-2.0	0.06
0.0-0.2	0.97
0.2-0.4	0.93
0.4-0.6	0.82
0.6-0.8	0.76
0.8-1.0	0.71

Table IV. Correlation of Fused Silica and Snow Silica Reduced Intensity Functions, $s_i(s)$

Range (nm)	Correlation
0.0-1.5	0.83
0.0-0.5	0.85
0.5-1.0	0.77
1.0-1.5	0.86
0.1-0.3	0.73
0.3-0.6	0.83
0.6-0.9	0.87
0.9-1.2	0.78
1.2-1.5	0.87

proximately four Si-O stretches, three O-Si-O bends, and two Si-O-Si bends.

The potential energy associated with each displacement x (in nanometers) from the equilibrium distance may be expressed in terms of the force constant, k (in mdyn/nm), for that displacement.

$$U \text{ (kJ/mol)} = (3.010 \times 10^{-9})kx^2 \quad (6)$$

Assuming a normal distribution with variance l^2 (in nm²), we may integrate over the distribution to give the total potential energy

$$U \text{ (kJ/mol)} = (3.010 \times 10^{-9})kl^2 \quad (7)$$

The potential energy difference between the two phases associated with each type of distance distribution may then be expressed as

$$\Delta U \text{ (kJ/mol)} = (3.010 \times 10^{-9})k\Delta l^2 \quad (8)$$

where Δl^2 is the difference in variances for the disorder distributions of snow and fused silica.

(7) Potential Energy Difference in Si-O Distributions

The thermal motion distributions were assumed to be the same for the two phases. The difference in the variances of disorder distributions is then the difference in the experimental distributions $\Delta l = (0.0067 \text{ nm})^2 - (0.0056 \text{ nm})^2$. Thus, using $k(\text{Si-O stretch}) = 74.76 \text{ mdyn/nm}$, one obtains

$$U_{\text{snow}} - U_{\text{fused}} = 3.0 \pm 0.2 \text{ kJ/mol} \quad (9)$$

for each Si-O distortion mode. Therefore, we associate (4) (3.0) = 12.0 \pm 0.8 kJ/mol of instability with Si-O distortions.

(8) Potential Energy Difference in O-O Distributions

A similar analysis may be carried out on the O-O distributions. This distribution involves both Si-O stretches and O-Si-O bends. The variance of the positional disorder distribution is taken to be the sum of contributions from two uncorrelated Si-O stretch distributions and one O-Si-O bend. The stretch is along the Si-O bond, whereas the bending component for the oxygen atoms is perpendicular. This being the case, the Si-O stretch contribution to the variance of the O-O distribution is approximately $\sin^2(\theta/2)$ times the variance of the Si-O distribution, where θ is the O-Si-O angle. The variance of the bend component that is perpendicular to the Si-O bonds must be multiplied by $\cos^2(\theta/2)$ to yield the variance of the bend distribution along the O-O direction.

The difference in variances for an O–Si–O bend is then approximated by

$$\begin{aligned}\Delta I_{\text{O-O}}^2 &= [\Delta I_{\text{O-O}}^2 - 2 \sin^2(\theta/2) \Delta I_{\text{Si-O}}^2] / \cos^2(\theta/2) \\ &= 8.85 \times 10^{-5} \text{ nm}^2\end{aligned}\quad (10)$$

Using $k(\text{O–Si–O bend}) = 10.0 \text{ mdyn/nm}$

$$U_{\text{snow}} - U_{\text{fused}} = 6.9 \pm 2.6 \text{ kJ/mol}$$

for each O–O distortion mode. Therefore, we associate (3) (6.9) = 20.7 \pm 7.8 kJ/mol destabilization with O–O distortions.

(9) Potential Energy Difference in Si–Si Distributions

In the same way as for the O–O distribution, we calculate the differences in variances for the Si–O–Si bend to be

$$\Delta I_{\text{Si-Si}}^2 = 5.47 \times 10^{-4} \text{ \AA}^2\quad (11)$$

Using a force constant of 1.0 mdyn/nm, the potential energy difference is

$$U_{\text{snow}} - U_{\text{fused}} = 4.3 \pm 1.60 \text{ kJ/mol}$$

for each Si–Si distortion mode. Therefore, we associate 8.6 \pm 3.2 kJ/mol instability with the two modes.

The calculated contributions to the excess energy are 12.0 kJ for Si–O bond length distortions, 20.7 kJ for distortions of the O–Si–O angles in the SiO₄ tetrahedra, and 8.6 kJ from Si–Si distortions leading to changes in the distribution of Si–O–Si angles, or a total of 41.3 kJ/mol. The largest energy contribution comes from the O–O distortions, which result in a significantly different mean O–Si–O angle for snow (107.8° \pm 0.5°) than for bulk glass (109.9° \pm 0.4°). The smaller energy terms arise from differences in Si–O and Si–Si distributions which do not significantly change the mean values but substantially increase the variance in the Si–O distances ((0.0067 nm)² in snow, (0.0056 nm)² in fused glass) and of the Si–Si distance ((0.0130 nm)² in snow, (0.01 nm)² in fused glass). The molecular orbital calculations of Gibbs⁸ as well as comparisons with bond length and bond angle variations in crystalline silicates suggest that it costs less energy to change bond angles than to alter the Si–O bond length. The results here suggest that the total energetic contributions reflect a balance between the energy needed for a given distortion (the force constants used in the calculations above) and the extent to which that distribution differs from snow to glass. Although the force constants and energy calculations used cannot represent a unique set of parameters, the conclusion that the major distortions and the major source of excess energy come from bond bending rather than from changes in Si–O distances appears reasonable and lends support to the approach used. It is interesting that the data suggest a greater distortion within SiO₄ tetrahedra (change in average O–Si–O angle and its variance) than in Si–O bond length and Si–O–Si angles (average values unchanged though variance increased) and that the largest energy increment is associated with the former.

For chemically vapor deposited SiO₂ films, Huffman and McMillan¹¹ interpret their Raman data to suggest a smaller average Si–O–Si angle in deposited films than in annealed films or bulk glass. No comparable Raman spectrum could be obtained for snow samples because of strong surface scattering (consistent with the morphology seen by SEM³) and the voids inferred from SAS in this study). Both films and snow were found to contain significant amounts of Si–H and Si–OH species which disappear on annealing. These may be related to some of the differences seen in the Si–O, Si–Si, and O–O distributions. Perhaps distorted O–Si–O angles are found in tetrahedra containing H or OH species and not linked to four other tetrahedra through Si–O–Si bonds. Such “defects” may also contribute to the energetics, but although their concentration cannot be readily quantified, it is unlikely to be high enough to contribute a large fraction of the total stored energy.³

From this study the following conclusions can be drawn. The snow contains a distribution of voids and/or particles but it is unlikely that the surface energy terms contribute more than 10% to 20% of the total excess energy. The RDFs of snow and fused silica are rather different. The snow has a wider distribution of Si–O, O–O, and Si–Si distances and far less order at distances beyond 1.0 nm than does bulk glass. Though the mean Si–O distance and the Si–O–Si angles in snow and glass are the same within experimental error, the average of the O–Si–O angles within the SiO₄ tetrahedra are smaller for snow than for glass. The total excess energy using a simple potential energy model for these distortions is in good agreement (41.3 \pm 7.9 kJ/mol) with that measured by calorimetry (46.9 \pm 0.8 kJ/mol). The major contribution to this excess energy comes from changes in bond angle distributions.

Acknowledgment: We thank F.S. Pintchovski for encouragement and discussion.

References

- ¹Thin Film Processes. Edited by J. L. Vossen and W. Kern. Academic Press, New York, 1978.
- ²A. M. Levelut and A. Guinier, “X-ray Scattering at Low Angles by Homogeneous Substances” (in Fr.), *Bull. Soc. Fr. Mineral. Cristallogr.*, **90**, 445 (1967).
- ³M. Huffman, A. Navrotsky, and F. S. Pintchovski, “Thermochemical and Spectroscopic Studies of Chemically Vapor Deposited Amorphous Silica,” *J. Electrochem. Soc.*, **133** [1] 164 (1986).
- ⁴O. Kratky, I. Pilz, and P. J. Schmitz, “Absolute Intensity Measurement of Small Angle X-ray Scattering by Means of a Standard Sample,” *J. Colloid Interface Sci.*, **21**, 24–34 (1966).
- ⁵A. Guinier, G. Fournet, C. B. Walker, and K. L. Yudowitch, *Small Angle Scattering of X-rays*. Wiley, New York, 1955.
- ⁶J. H. Konnert and J. Karle, “The Computation of Radial Distribution Functions for Glassy Materials,” *Acta Crystallogr., Sect. A*, **29**, 702 (1973).
- ⁷J. H. Konnert, P. D’Antonio, and J. Karle, “Comparison of Radial Distribution Function for Silica Glass with Those for Various Bonding Topologies,” *J. Non-Cryst. Solids*, **53**, 135–41 (1982).
- ⁸D. Kuhl and R. L. Hildebrand, Program SPEC, Chemistry Department, University of Texas, 1976.
- ⁹G. V. Gibbs, “Molecules as Models for Bonding in Silicates,” *Am. Mineral.*, **67**, 425–50 (1982).
- ¹⁰J. H. Konnert and D. E. Appleman, “The Crystal Structure of Low Tridymite,” *Acta Crystallogr., Sect. B*, **34**, 391 (1978).
- ¹¹M. Huffman and P. McMillan, “Infrared and Raman Studies of Chemically Vapor Deposited Amorphous Silica,” *J. Non-Cryst. Solids*, **76**, 369 (1985). □